Entropy in Molecular Fluids: Interplay between Interaction Complexity and Criticality

Caroline Desgranges and Jerome Delhommelle*

Department of Chemistry, New York University, New York, New York 10003, United States & Department of Chemistry & Molecular Simulation of NonEquilibrium Processes (MSNEP), Suite 2300, Tech Accelerator, University of North Dakota, Grand Forks, North Dakota 58202, United States

E-mail: jerome.delhommelle@und.edu

*To whom correspondence should be addressed

Abstract

Using flat-histogram simulations, we calculate the entropy of molecular fluids along the vapor-liquid phase boundary. Our simulation approach is based on the evaluation of the canonical and grand-canonical partition functions, which, in turn, provide access to entropy through the statistical mechanics formalism. The results allow us to determine the critical entropy of molecular fluids and to uncover that the transition occurs symmetrically from an entropic standpoint. This can best be seen through the patterns exhibited by the thermodynamic variables temperature and pressure when plotted against the entropy of the coexisting phases. This behavior is found to hold for apolar, quadrupolar and dipolar fluids. Finally, we identify functional forms that characterize the relation between thermodynamic variables and entropy along the coexistence curve up to the critical point.

Introduction

Entropy is notoriously challenging to calculate.[1] This property, however, is essential to detect the onset of order↔disorder transitions. Furthermore, since entropy is one of the partial derivatives of the Gibbs free energy, it can be used to characterize a phase transition in the Ehrenfest classification[2] through either its non-continuous (first order) or continuous (second order) behavior. This has prompted the development of several different strategies to determine entropy. A possible route to its calculation is through a thermodynamic approach and the use of the well-known thermodynamic relation $S = \frac{H-G}{T}$. However, obtaining an accurate value for the Gibbs free energy G can present significant challenges. A way to achieve this is by carrying out molecular simulations in the grand-canonical ensemble,[3–7] in which μ is fixed and N is allowed to fluctuate. Another approach consists in computing μ via the method designed by Widom,[8] *i.e.* by inserting a test particle in the system during the simulations.[9–16] This second method is applicable to simulations in the canonical or isothermal-isobaric ensemble, for which the total number of molecules N is fixed. Both techniques then allow to calculate S as $\langle S\rangle = \frac{\langle H\rangle - \mu\langle N\rangle}{T}$ in the (μ,V,T) ensemble, or $\langle S\rangle = \frac{\langle H\rangle - \langle\mu\rangle N}{T}$ in the (N,V,T) or (N,P,T) ensembles, with $\langle . \rangle$ denoting ensemble averages. How-

ever, such approaches become less accurate as the density increases or as the molecular geometry becomes more complex, given the low acceptance rates for random insertions. In such cases, the determination of the Gibbs free energy, and thus of the entropy, requires more elaborate strategies, for instance, by starting from a reference state of known G and connecting it to the system of interest along a thermodynamic path via thermodynamic integration[17–20] or using Bennett acceptance ratio.[21] Another alternative consists in leveraging configurational bias Monte Carlo (MC) moves[22] or Expanded Ensemble methods[23,24] to gradually insert/delete molecules in the system and bolster the acceptance rates for such MC moves.

Another possible route to calculate S is through the use of structural information. Entropy can be cast into a sum of one-body, two-body, three-body... contributions[25,26] $S/Nk = s^{(0)} + s^{(2)} + s^{(3)} + ...$ and calculated through the Green-Wallace[10,27–29] expansion in terms of the multiparticle correlation functions. This approach has been successfully applied to determine the entropy of atomic fluids.[30–33] Furthermore, through the two-body approximation, it has also been used to study water and waterlike anomalies,[34–37] to examine ordering in liquids,[38–42] to calculate the entropy of hydrophobic hydration[43–45] and to model molecular recognition in protein-ligand binding.[46,47] However, this approach remains challenging to apply to complex molecules and at high densities, since, in this case, the three-body, and more generally the many-body contributions, become non-negligible.[25,48] Alternatively, dynamical information can be used to calculate the entropy of a molecular fluid through a Fourier transform of the velocity autocorrelation function.[49,50]

Here, we focus on a statistical mechanical approach to calculate the entropy and to shed light on the behavior of entropy along a phase boundary, as recent observations on atomic fluids[51] have suggested that, unlike other thermodynamic properties, entropy could exhibit a symmetric behavior along a coexistence curve. Our approach is based on the determination of the partition function $\Theta(\mu, V, T)$ via the extensive sampling of the configurational space using the Expanded Wang-Landau (EWL) simulation method.[52–56] This relies on a flat histogram sampling method, known as the Wang-Landau sampling,[57–62] combined with an expanded ensemble approach[63–69] to bolster the acceptance rate of random insertion/deletion and handle large molecules, and high

density states. Once an accurate estimate for the partition function has been obtained, S can then be evaluated through

$$S = \frac{k_B \ln \Theta(\mu, V, T)}{< N >} + \frac{< U > -\mu}{T} \tag{1}$$

in which $< N >$ and $< U >$ are collected during the simulations, and S and U denote intensive properties.

The goal of this work is to use this statistical mechanical approach to calculate the entropy of molecular fluids along the vapor-liquid phase boundary for molecular fluids. The questions we aim to address here are the following: (i) can we determine an estimate for the critical entropy S_c of molecular fluids? (ii) does the symmetry observed in prior work on atomic systems also apply to molecular fluids? (iii) what is the impact of the increase in the complexity and range of the intermolecular interactions, *e.g.*, by taking into account the effect of permanent electrostatic moments such as quadrupoles (as in N_2 and CO_2) or dipoles (as in H_2O)? and (iv) can we identify a pattern for the entropy at coexistence that remains valid for apolar, quadrupolar and dipolar molecular fluids? To address these issues, we carry out EWL simulations to calculate the entropy along the vapor-liquid coexistence curves for a series of molecular fluids, starting from apolar (SF_6) to quadrupolar (N_2 and CO_2) and finally to dipolar (H_2O) molecules. We compare the simulation results to the available experimental data and determine the location of the critical point, including the critical entropy S_c. We then scale the thermodynamic properties with respect to the coordinates of the critical point to identify a behavior common to these systems and to provide a full picture of the phase transition from an entropic standpoint.

The paper is organized as follows. We first provide an account of the force fields used to model the different molecules studied in this work. We briefly discuss the EWL algorithm used in this work to calculate the entropy of molecules. We then present results for the vapor-liquid equilibria, compare them to the available data and examine the dependence of entropy upon the interaction complexity through scaled temperature-entropy and pressure-entropy. We finally draw the main conclusions from this work in the last section.

Simulation method and models

Force Fields

We use different force fields to model the molecules studied in this work. These force fields were chosen for their ability to provide simulation results in very good agreement with the experimental data for the densities of the two coexisting phases, for the temperature dependence of the saturation pressure and for the location of the critical point (T_c, ρ_c, P_c).

We model the non-polar SF_6 molecule with 6 interaction sites placed on each of the F atoms of the molecule. Interaction sites located on two different molecules interact through the Lennard-Jones (LJ) potential form as follows

$$U(r_{ij}) = 4\varepsilon_{ij}\left[\left(\frac{\sigma_{ij}}{r_{ij}}\right)^{12} - \left(\frac{\sigma_{ij}}{r_{ij}}\right)^{6}\right] \tag{2}$$

with r_{ij}, σ_{ij} and ε_{ij} the LJ parameters between two interactions sites. The distance between the center of mass (S atom) and each of the F atoms is set to 1.62 Å and the LJ parameters[70] are set to $\sigma = 2.75$ Å and $\frac{\varepsilon}{kB} = 78$ K.

For the quadrupolar nitrogen N_2 molecule, we use a force field consisting of a distribution of point charges and of two LJ sites on the two N atoms. The overall interaction can be written as

$$U(r_{ij}) = 4\varepsilon_{ij}\left[\left(\frac{\sigma_{ij}}{r_{ij}}\right)^{12} - \left(\frac{\sigma_{ij}}{r_{ij}}\right)^{6}\right] + \frac{q_i q_j}{4\pi\varepsilon_0 r_{ij}} \tag{3}$$

with the following LJ parameters for the N atoms $\sigma = 3.3$ Å and $\frac{\varepsilon}{kB} = 36$ K. In this force field, the bondlength $N-N$ is equal to 1.098 Å. The three point charges are fitted to model the quadrupole of N_2. A single positive charge (0.966 e) is placed at the center of $N-N$ bond, while the two negative charges (-0.483 e) are located on the two N atoms.[71] The quadrupolar carbon dioxide CO_2 molecule is modeled with the TraPPE force field.[72] It consists of three LJ sites and three point charges located on each of the atoms. The molecule is taken as rigid with a bondlength for C-O of 1.16 Å and a bond angle for $\angle$OCO of 180^0. The parameters are $\sigma_C = 2.8$ Å and $\frac{\varepsilon_C}{kB} = 27$ K,

$\sigma_O = 3.05$ Å and $\frac{\varepsilon_O}{kB} = 79$ K, $q_C = 0.7$ e and $q_O = -0.35$ e. The interactions between unlike atoms are obtained via the Lorentz-Berthelot combining rules.[73]

We use the SPC/E force field to model the dipolar water molecule.[74] This force field provides a very good account of the vapor-liquid equilibria properties of water.[15,75,76] It includes three interaction sites, with a single LJ site on the O atom and point charges on each of the atoms. The model assumes the molecule to be rigid with a O-H bondlength of 1 Å and an angle for $\angle$HOH of 109.47^0. For the LJ site, we have $\sigma_O = 3.166$ Å and $\frac{\varepsilon_O}{kB} = 0.65$ kJ/mol. The point charge on O is equal to $q_O = -0.8476$ e, while for the two H atoms $q_H = 0.4238$ e.

Simulation framework

To compute entropy, we calculate the canonical and grand-canonical partition functions. A versatile and highly accurate method to determine partition functions in isothermal ensembles is the Wang-Landau sampling method.[57–62] Since we focus here on vapor liquid equilibria, we use the expanded Wang-Landau (EWL) method.[52–56] In this approach, the insertion/deletion of molecules is split into a finite number of stages according to the expanded ensemble method.[63–69] This means that the Monte Carlo (MC) steps corresponding to random insertions and deletions are replaced by MC steps in which a fractional molecule is grown/shrunk until a new molecule has formed in/disappeared from the system. This bolsters the acceptance rate for the MC moves and leads to accurate partition functions for atomic and molecular systems, including for high density liquids.[52] This method is a flat histogram simulation approach, meaning that an extensive sampling of N, the number of molecules, that can fit within a volume V and at a temperature T is carried out (flat histogram for the number of visits), and that the partition function is dynamically updated during the EWL simulations until convergence has been reached. The output of EWL simulations are the grand-canonical partition function $\Theta(\mu,V,T)$ and the canonical partition function $Q(\mu,V,T)$, which are related through

$$\Theta(\mu,V,T) = \sum_{N=0}^{\infty} Q(N,V,T)\exp(\beta\mu N) \tag{4}$$

Entropy can then be obtained using Eq. 1 as discussed in the Introduction. We detail below how $< N >$ and $< U >$ are obtained from the EWL simulations. Starting from the probability distribution $p(N)$ defined as

$$p(N) = \frac{Q(N,V,T)\exp(\beta\mu N)}{\Theta(\mu,V,T)} \tag{5}$$

the average number of molecules can be obtained through

$$\langle N \rangle = \sum p(N)N \tag{6}$$

The average internal energy then follows from

$$< U >= \sum_{N} (E_{pot}(N) + E_{kin})p(N) \tag{7}$$

in which E_{pot} and E_{kin} are the average potential energy and kinetic energy, respectively, calculated for a given (N,V,T) set. E_{pot} is calculated during the simulations as the total interaction energy between molecules and $E_{kin} = \frac{N_f}{2} k_B T$ is a function of the number of degrees of freedom N_f in the model, *e.g.* $N_f = 5$ for a linear molecule like N_2 or CO_2 and $N_f = 6$ for a non-linear molecule like SF_6.

Technical details

The EWL simulations rely on an iterative process, that collects histograms for the number of visits for each N sampled and for the value of $Q(N,V,T)$ every time a configuration for a specific value of N is visited. From a practical standpoint, given the large values taken by $Q(N,V,T)$, we store an histogram for $\ln Q(N,V,T)$ rather than of $Q(N,V,T)$. Every time a value of N is visited, the number of visits for N is incremented by 1 and the histogram for $\ln Q(N,V,T)$ is incremented by $\ln f$, in which f denotes the convergence factor. The criterium for the minimum number of visits is set to 1000 for all N. Every time this criterion is satisfied, the histogram for the number of visits is reset to 0 and the convergence factor is reduced to $\sqrt{f}$ until it becomes less than 10^{-8} (its initial value is

set to $\ln f = 1$ as in previous work[52,54]). The number of stages, in which the insertion/deletion of a molecule is split, is set to 100 for all systems. For all systems, MC steps are attempted according to the following probabilities: 37.5% for translations of a molecules, 37.5% for rotations and 25 % for growth/shrinkage. Finally, we use a spherical cutoff, set to half the boxlength, for the calculations of LJ interactions, and apply tail corrections[73] beyond. Ewald sums are used to calculate the long-range Coulombic interactions, with a screening parameter for the charge Gaussian distribution of $5.6/L$ and a reciprocal cutoff vector of $k_{max} = 6(2\pi)/L$.

Results and discussions

We first present the results for the grand-canonical partition function for N_2, and show on this example how the evaluation of $\Theta(\mu,V,T)$ allows us to carry out the calculation of the entropy. We start by showing in Fig. 1(a) the canonical partition function $Q(N,V,T)$ for $T = 110$ K and for $N = 0$ to $N = 460$, *i.e.* for numbers of molecules encompassing densities ranging from the vapor to the liquid phase. The shape of the plot obtained here is consistent with that found for subcritical fluids,[69] with an increase in $Q(N,V,T)$ from its initial value of 1 for a system containing 0 molecule to the very values obtained close to the upper bound for N. The simulation results can then be used to compute the grand-canonical partition function $\Theta(\mu,V,T)$ for any value of the chemical potential μ through Eq. 4. The results are also shown in Fig. 1(a) and indicate that there is a sharp change in $\ln\Theta(\mu,V,T)$ characteristic of the onset of a phase transition, and specifically here of the vapor-liquid transition for a chemical potential $\mu = -440.39$ kJ/kg, in very good agreement with the experimental data[77] of -444.65 kJ/kg. The value of $\ln\Theta(\mu,V,T)$ at this juncture can also be used to calculate the pressure at coexistence through the relation

$$P = \frac{k_B T \ln\Theta(\mu,V,T)}{V} \tag{8}$$

We find a value of $P = 16.75$ bar from the EWL simulation results, in very good agreement with the experimental value[77] of $P = 14.67$ bar. This establishes the accuracy of the partition functions,

and of the thermodynamic pressure, obtained from the EWL simulations.

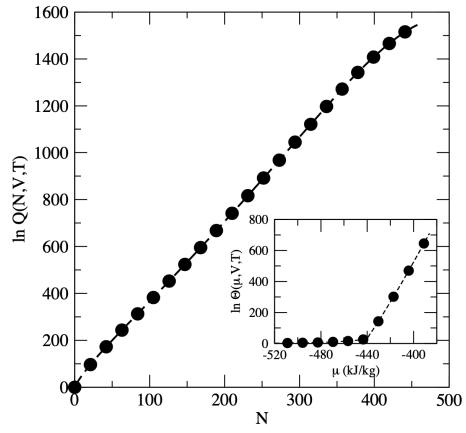

(a)

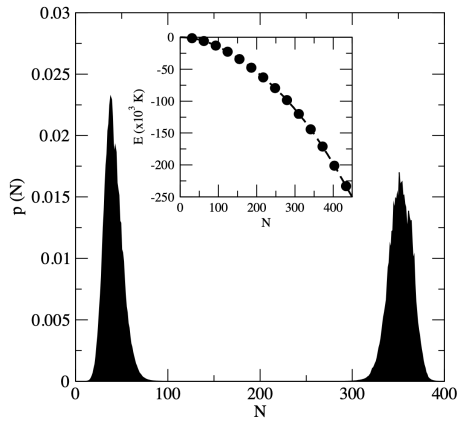

(b)

Figure 1: N_2 at $T = 110$ K. (a) Logarithm of the canonical partition function $\ln Q(N,V,T)$ as a function of the number of molecules N. The inset shows the variation of $\ln \Theta(\mu,V,T)$ with the chemical potential μ. (b) Probability distribution at coexistence for the vapor and the liquid phases. The inset is a plot of the potential energy versus N.

To analyze further the results and obtain the remaining properties at coexistence, we calculate the probability distribution for N using Eq. 5. We plot in Fig. 1(b) the variations of $p(N)$ as a function of N at coexistence. We observe two peaks of equal area, with the peak on the left of the graph corresponding to the vapor phase and the peak on the right corresponding to the liquid. Using the statistical mechanics formalism, we can compute the densities at coexistence from the probability distribution as $\rho = \sum_N \frac{N}{V} p(N)$ over each of the two peaks. At coexistence, the $p(N)$ distribution exhibits a minimum between the two peaks for a value of $N = N_b$. In line with prior work,[52] we compute the properties using the probability distribution $p(N)$ for values of N up to

N_b in the case of the vapor phase, and for values of N greater than N_b for the liquid phase. We find that $\rho_l = 0.607$ g/cm^3 and $\rho_v = 0.071$ g/cm^3 from the EWL simulation results. These results are found to be, once again, in very good agreement with experimental data[77] ($\rho_l = 0.626$ g/cm^3 and $\rho_v = 0.063$ g/cm^3). We also plot (inset of Fig. 1(b)) the dependence of the potential energy of the fluid as a function of N as collected during the EWL simulations. This is the last piece of information necessary to calculate the entropy through Eq. 1.

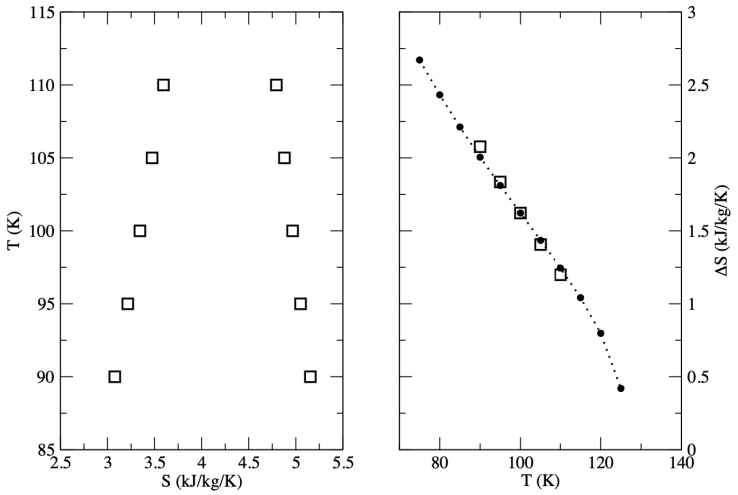

Figure 2: (Left) Entropy for the liquid (low S) and the vapor (high S) along the phase boundary for N_2. (Right) $\Delta S = S_v - S_l$ as a function of temperature. EWL results are shown as squares, while experimental data[77] are plotted as filled circles and connected with a dotted line for eye guidance.

Gathering the EWL simulation results at coexistence for $\Theta(\mu, V, T)$, for the average numbers of molecules and energy of each of the two phase, we can evaluate the entropy for the two coexisting phases. We plot the results against temperature in the left panel of Fig. 2 for the liquid and the vapor branches for N_2. We observe that, as temperature increases, the entropy of the liquid increases, while the entropy for the vapor phase decreases. This is consistent with the expected trend for the densities, namely that the density of the liquid at coexistence decreases as temperature increases, leading to a greater entropy. Conversely, the density of the vapor increases along the phase

boundary as temperature increases, leading to a lower entropy. The right panel of Fig. 2 shows the difference in entropy between the two phases, together with a comparison with the experimental data.[77] As a result of the combined variations in S_l and S_v, ΔS decreases as the temperature increases. For instance, we find from the EWL simulation results a value of $\Delta S = 1.20$ kJ/kg at $T = 110$ K, in very good agreement with the experimental data[77] ($\Delta S = 1.25$ kJ/kg). This validates the statistical mechanical approach used in this work to calculate the entropy at coexistence, as well as the accuracy of the EWL simulations and of the partition functions $Q(N,V,T)$ and $\Theta(\mu,V,T)$.

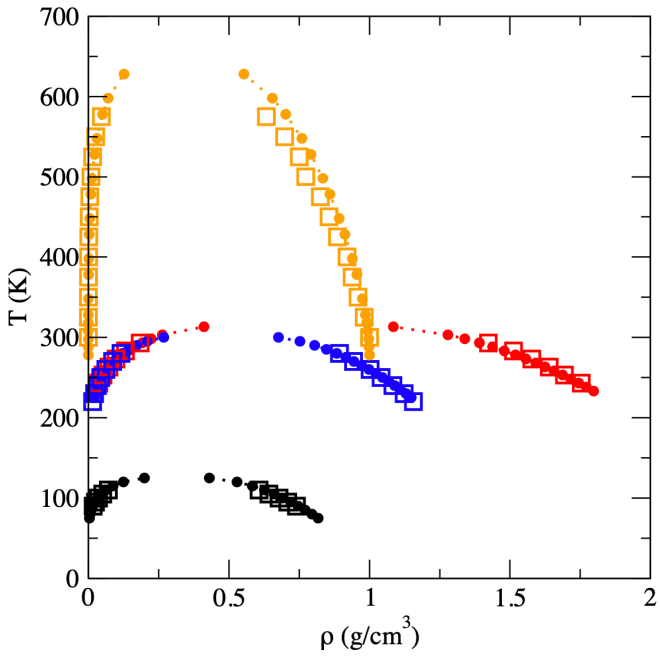

Figure 3: Vapor-liquid equilibria for SF_6 (red), N_2 (black), CO_2 (blue) and H_2O (orange). Experimental data[77,78] are shown as filled circles, while EWL simulation results are shown with open squares.

We now turn to the results obtained for the phase envelope of the various molecular fluids considered here. We report in Fig. 3 the results obtained from the EWL simulations, together with the experimental data from the literature.[77,78] For all systems, the simulated vapor-liquid equilibria are in good agreement with the experimental data. This shows that the force fields used in this work provide a very good account of the features of the vapor-liquid phase transition for this series of molecular fluids.

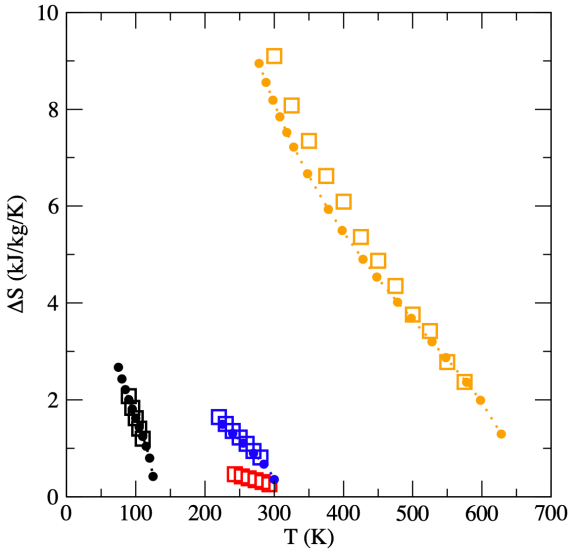

Figure 4: Dependence of ΔS as a function of temperature. Same legend as in Fig. 3.

The variation of ΔS as a function of temperature for all the molecules studied in this work is plotted in Fig. 4. Since experimental data is available for all systems on ΔS (with the exception of SF_6), this allows us to test the ability of the force fields and of the EWL simulations to account correctly for the entropy change as the system undergoes the phase transition process. The comparison between simulations and experiments is plotted in Fig. 4. This shows that our approach provides accurate results for entropy along the phase boundary of molecular systems, and that it accounts correctly for the various types of intermolecular interactions considered in this work.

To compare the behavior of the entropy along the phase boundary, we rescale the properties for each fluid by its critical properties and compare the scaled entropy-pressure and entropy-temperature plots along the phase boundary. Thus, the next step consists in evaluating the critical properties for all systems. To this end, we build on the standard scaling laws to determine the thermodynamic locus for the critical point. Starting with the critical temperature, we extrapolate

T_c through the following scaling law applied to the order parameter $\rho_l - \rho_v$

$$\rho_l - \rho_v = B(T - T_c)^{\beta} \tag{9}$$

in which $\beta = 0.325$ is the 3D Ising exponent and B and T_c are two fitting parameters. To determine the critical density ρ_c, we use the law of rectilinear diameters[79]

$$\frac{\rho_l + \rho_v}{2} = \rho_c + A(T - T_c) \tag{10}$$

in which A and ρ_c are two fitting parameters. The critical pressure P_c is obtained by fitting the simulation results with the Antoine equation

$$\ln P = C - \frac{D}{T + E} \tag{11}$$

in which C, D and E are fitting parameters, and finding the value taken by pressure at $T = T_c$. Finally, we calculate the critical entropy by taking the average of the entropy for the two coexisting phases at the highest temperature available. As we will see in the next paragraph, the highly symmetric behavior of the entropy along the phase boundary is a sound basis for the evaluation of S_c through a simple arithmetic average. We summarize in Table 1 the results for the critical points, as well as the available experimental critical points, for the molecules studied in this work. The estimates for the critical temperature, critical pressure and critical density from the simulation results are in very good agreement with the experimental data for all systems, further confirming that the force fields perform well for all molecules considered here and that EWL simulations are an accurate approach for the determination of the critical properties. Here, the novel information provided by EWL simulations is the estimate for the critical entropy S_c for these systems. Experimental data for S_c is available for N_2 and CO_2 and provides a direct test. Indeed, we find that the value of S_c obtained from EWL simulations is within 1.4% of the experiment for N_2 and 2.2% in the case of CO_2, which shows that our approach yields accurate results for S_c.

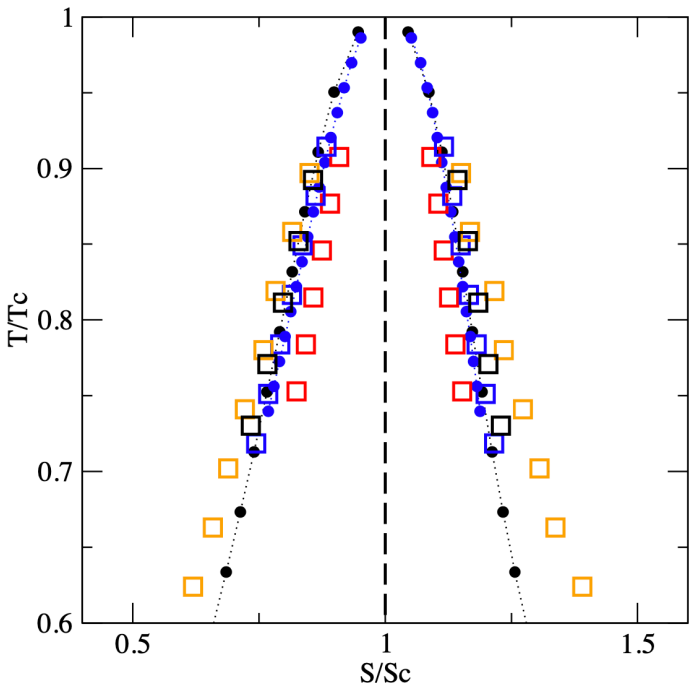

Figure 5: Scaled temperature-entropy plot along the phase boundary for the liquid (low entropy) branch and the vapor (high entropy) branch. Same legend as in Fig. 3.

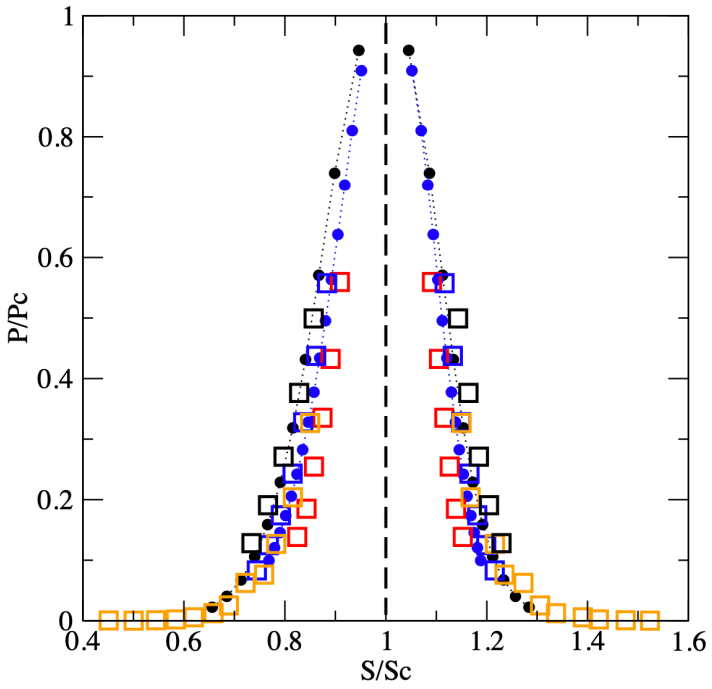

Figure 6: Scaled pressure-entropy plot along the phase boundary for the liquid (low entropy) branch and the vapor (high entropy) branch. Same legend as in Fig. 3.

Table 1: Critical properties for the molecular fluids studied in this work. EWL denotes the Expanded Wang-Landau simulation results, and Exp the experimental data.[77,78]

	SF_6	N_2	CO_2	H_2O
T_c EWL (K)	323	123	306	641
T_c Exp (K)	319	126	304	647
P_c EWL (bar)	39.1	33.5	75.8	223.8
P_c Exp (bar)	38.8	34.0	73.8	220.6
ρ_c EWL (g/cm^3)	0.75	0.31	0.47	0.31
ρ_c Exp (g/cm^3)	0.74	0.31	0.47	0.32
S_c EWL (kJ/kg/K)	1.42	4.19	3.49	7.90
S_c Exp (kJ/kg/K)	-	4.25	3.57	-

We gather in Fig. 5 the scaled temperature-entropy plots for all compounds considered here. The graph shows two branches: one for the liquid, or low entropy branch, and one for the vapor, or high entropy branch. The plot also shows that the two entropy branches close at the critical point of coordinate $(1,1)$ in the scaled plots. Very interestingly, despite the significant differences between the types of intermolecular interaction that take place in these systems, the scaled plots exhibit two remarkable features. First, they show a highly symmetric behavior, regardless of whether the molecules bear a permanent dipole, quadrupole or a higher electrostatic moment. To better assess this symmetry, we consider the equation $\frac{(S_l+S_v)}{2} = S_c + A(T-T_c)$ and fit the data to determine the fitting parameter A. We obtain very small values for A, ranging from 10^{-3} to 10^{-4} for all systems, and with p values ranging from 10^{-3} to 10^{-7}. This provides numerical evidence for the determination of S_c and for the symmetric behavior observed for the entropy along the binodal. Second, the plots for the various compounds nearly fall exactly onto the same plot. This suggests that a behavior, akin to what is observed for the law of corresponding states, can be observed for these entropic plots of the phase coexistence curves. Focusing on the results obtained for temperatures close enough to the critical point, we carry out fits for temperatures such that $T/T_c > 0.75$ for the liquid branch according to

$$\frac{T}{T_c} = A_l(1-\frac{S_l}{S_c})^{\upsilon_l} + 1 \tag{12}$$

and for the vapor branch

$$\frac{T}{T_c} = A_v(\frac{S_v}{S_c} - 1)^{\upsilon_v} + 1 \tag{13}$$

in which A_l, A_v, υ_l and υ_v are fitting parameters. We gather the results in two groups. The first group includes the experimental data, which only accounts for N_2 and CO_2 since these are the two systems for which we have S_c^{exp}. The second group includes the EWL simulation results for all systems and all types of interactions studied here. Allowing for υ_l and υ_v to take different values and thus allowing for an asymmetric entropic behavior, we find that $\upsilon_v = 1.95$ and $\upsilon_l = 1.61$ lead to entropies within a root-mean square error (RMSE) of 0.009 with respect to the data for the experimental group, and with a RMSE of 0.076 for the EWL group. The larger RMSE for the EWL group is consistent with the much broader range of compounds, and of intermolecular interaction types, accounted for in the second group. Constraining $\upsilon_v = \upsilon_l$ (assuming a symmetric behavior) leads to an exponent of 1.78. We add that with this exponent we obtain similar RMSEs as when we allow for $\upsilon_v \neq \upsilon_l$, both for the experimental group (0.010) and for the EWL group (0.081). This implies that this constraint does not impact significantly the accuracy of the fit, and thus confirms the symmetric nature of the scaled temperature-entropy plot.

Turning now to the scaled pressure-entropy plot in Fig. 6, we find that the two branches for the liquid and for the vapor also exhibit a symmetric in line with our findings for the scaled temperature-entropy plots shown in Fig. 5. We therefore follow the same method as before to analyze the results. More specifically, we focus on the results obtained as the system approaches criticality, and here include data for $P/P_c > 0.3$, and perform the following fits for the two groups

$$\begin{aligned} \frac{P}{P_c} &= C_l(1 - \frac{S_l}{S_c})^{\omega_l} + 1 \\ \frac{P}{P_c} &= C_v(\frac{S_v}{S_c} - 1)^{\omega_v} + 1 \end{aligned} \tag{14}$$

in which C_l, C_v, ω_l and ω_v are fitting parameters. Given the symmetric nature of the pressure-entropy plot, we constrain $\omega_l = \omega_v$ and find an optimal value of 1.24 for the exponent. This leads to an overall RMSE of 0.087 for the experimental group and of 0.221 for the EWL group. We

obtain again a larger RMSE for the EWL group, as expected from the much broader range of compounds and of interaction types taken into account in this group.

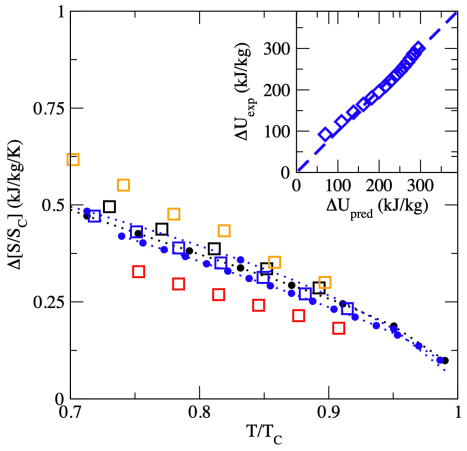

Figure 7: Scaled entropy of vaporization-temperature plot along the phase boundary for the systems studied in this work. Same legend as in Fig. 3. (Inset) Experimental data for the internal energy of vaporization vs. values predicted using Eq. 16 for CO_2.

We now turn to the variation of the scaled entropy of vaporization as a function of the scaled temperature (see Fig. 7). From Eqs. 12 and 13, we can obtain the following relation between the scaled entropy of vaporization $\frac{\Delta S}{S_c} = \frac{[S_v - S_l]}{S_c}$ and temperature as

$$\frac{\Delta S}{S_c} = A\left(\frac{T_c - T}{T_c}\right)^{\zeta} \tag{15}$$

with $\zeta = \frac{1}{\upsilon}$, where υ is the exponent obtained from the fits of the data to Eqs. 12 and 13. Taking the value obtained previously ($\upsilon = 1.78$), we check that Eq. 15 accurately models the temperature dependence of ΔS, with, for instance, a RMSE of 0.008 for the experimental dataset for CO_2. We finally examine the variation of the internal energy of vaporization as a function of temperature. Using the thermodynamic definition for $S = \frac{P}{T\rho} + \frac{U}{T} - \frac{\mu}{T}$ for both phases at coexistence, we can write the internal energy of vaporization $\Delta U = U_v - U_l$ as

$$\Delta U = AS_cT\left(\frac{T_c - T}{T_c}\right)^{\zeta} - P\left(\frac{1}{\rho_v} - \frac{1}{\rho_l}\right) \tag{16}$$

in which we have replaced ΔS with the fit provided in Eq. 15. As shown in the inset of Fig. 7 on the example of CO_2, this equation models well the behavior of ΔU along the coexistence curve with a RMSE of less than 8 kJ/kg across the entire temperature range studied here.

Conclusions

In this work, we focus on the behavior of entropy along a phase boundary in a series of molecular fluids. The molecular fluids considered here (SF_6, N_2, CO_2 and H_2O) encompass several levels of interaction complexity, including systems solely relying on repulsion-dispersion, or short-range, interactions and systems with permanent quadrupoles and dipoles, leading to long-range interactions. This, in turn, allows us to assess the impact of the range and complexity of the intermolecular interactions on a recently observed symmetric behavior of entropy for the vapor-liquid equilibria of atomic fluids. To determine the entropy of molecular fluids along the phase boundary, we use a statistical mechanical approach, based on the evaluation of the canonical partition function and by the grand-canonical partition function through Expanded Wang-Landau simulations. Once the partition functions have been obtained, all thermodynamic properties, including the notoriously challenging determination of entropy, can be readily calculated. We test the EWL simulation results against the available experimental data for the entropy of the coexisting phases for N_2 and CO_2. We obtain a very good agreement between simulations and experiments for the variations of entropy along the phase coexistence, and for the change in entropy upon the phase change for N_2, CO_2 and H_2O. Our approach therefore allows us to determine the critical entropy S_c of molecular fluids for apolar, quadrupolar and dipolar systems. Further analysis on scaled temperature-entropy and pressure-entropy plots shows that, for all molecular systems, the phase transition occurs symmetrically from an entropic standpoint. We identify the values of the exponents according to which the two branches of the phase diagram close to reach the critical point. Extensions of this analysis to other types of systems, including, for instance, internal degrees of freedom and ionic fluids, will be the topic of future work.

Acknowledgements Partial funding for this research was provided by NSF through award CHE-1955403. This work used the Extreme Science and Engineering Discovery Environment (XSEDE),[80] which is supported by National Science Foundation grant number ACI-1548562, and used the Open Science Grid through allocation TG-CHE200063.

References

(1) Meirovitch, H. Recent developments in methodologies for calculating the entropy and free energy of biological systems by computer simulation. *Current Opinion Struct. Biol.* **2007**, *17*, 181–186.

(2) Ehrenfest, P. Phasenumwandlungen im ueblichen und erweiterten Sinn, classifiziert nach dem entsprechenden Singularitaeten des thermodynamischen Potentiales. *Verhandlingen der Koninklijke Akademie van Wetenschappen (Amsterdam)* **1933**, *36*.

(3) Adams, D. Grand canonical ensemble Monte Carlo for a Lennard-Jones fluid. *Mol. Phys.* **1975**, *29*, 307–311.

(4) Rowley, L.; Nicholson, D.; Parsonage, N. Monte Carlo grand canonical ensemble calculation in a gas-liquid transition region for 12-6 Argon. *J. Comput. Phys.* **1975**, *17*, 401–414.

(5) Mezei, M. Grand-canonical ensemble Monte Carlo study of dense liquid: Lennard-Jones, soft spheres and water. *Mol. Phys.* **1987**, *61*, 565–582.

(6) Whitley, H. D.; Smith, D. E. Free energy, energy, and entropy of swelling in Cs–, Na–, and Sr–montmorillonite clays. *J. Chem. Phys.* **2004**, *120*, 5387–5395.

(7) Puibasset, J. Grand potential, Helmholtz free energy, and entropy calculation in heterogeneous cylindrical pores by the grand canonical Monte Carlo simulation method. *J. Phys. Chem. B* **2005**, *109*, 480–487.

(8) Widom, B. Some topics in the theory of fluids. *J. Chem. Phys.* **1963**, *39*, 2808–2812.

(9) Powles, J. The liquid-vapour coexistence line by computer simulation à la Widom. *Mol. Phys.* **1980**, *41*, 715–727.

(10) Wallace, D. C. On the role of density fluctuations in the entropy of a fluid. *J. Chem. Phys.* **1987**, *87*, 2282–2284.

(11) Deitrick, G.; Scriven, L.; Davis, H. Efficient molecular simulation of chemical potentials. *J. Chem. Phys.* **1989**, *90*, 2370–2385.

(12) Nezbeda, I.; Kolafa, J. A new version of the insertion particle method for determining the chemical potential by Monte Carlo simulation. *Mol. Simulat.* **1991**, *5*, 391–403.

(13) de Pablo, J. J.; Laso, M.; Suter, U. W. Estimation of the chemical potential of chain molecules by simulation. *J. Chem. Phys.* **1992**, *96*, 6157–6162.

(14) Tamai, Y.; Tanaka, H.; Nakanishi, K. Molecular simulation of permeation of small penetrants through membranes. 2. Solubilities. *Macromolecules* **1995**, *28*, 2544–2554.

(15) Errington, J. R.; Boulougouris, G. C.; Economou, I. G.; Panagiotopoulos, A. Z.; Theodorou, D. N. Molecular simulation of phase equilibria for water- methane and water-ethane mixtures. *J. Phys. Chem. B* **1998**, *102*, 8865–8873.

(16) Schnabel, T.; Vrabec, J.; Hasse, H. Henry's law constants of methane, nitrogen, oxygen and carbon dioxide in ethanol from 273 to 498 K: Prediction from molecular simulation. *Fluid Phase Equilibr.* **2005**, *233*, 134–143.

(17) Lu, N.; Kofke, D. A. Accuracy of free-energy perturbation calculations in molecular simulation. I. Modeling. *J. Chem. Phys.* **2001**, *114*, 7303–7311.

(18) White, R. P.; Meirovitch, H. A simulation method for calculating the absolute entropy and free energy of fluids: Application to liquid argon and water. *Proc. Natl. Acad. Sci. U.S.A.* **2004**, *101*, 9235–9240.

(19) Cheluvaraja, S.; Meirovitch, H. Simulation method for calculating the entropy and free energy of peptides and proteins. *Proc. Natl. Acad. Sci. U.S.A.* **2004**, *101*, 9241–9246.

(20) Preisler, Z.; Dijkstra, M. Configurational entropy and effective temperature in systems of active Brownian particles. *Soft Matter* **2016**, *12*, 6043–6048.

(21) Bennett, C. H. Efficient estimation of free energy differences from Monte Carlo data. *J. Comp. Phys.* **1976**, *22*, 245–268.

(22) Siepmann, J. I.; Frenkel, D. Configurational bias Monte Carlo: a new sampling scheme for flexible chains. *Mol. Phys.* **1992**, *75*, 59–70.

(23) Escobedo, F. A.; de Pablo, J. J. Monte Carlo simulation of the chemical potential of polymers in an expanded ensemble. *J. Chem. Phys.* **1995**, *103*, 2703–2710.

(24) Martemyanova, J.; Stukan, M.; Ivanov, V.; Müller, M.; Paul, W.; Binder, K. Dense orientationally ordered states of a single semiflexible macromolecule: An expanded ensemble Monte Carlo simulation. *J. Chem. Phys.* **2005**, *122*, 174907.

(25) Baranyai, A.; Evans, D. J. Direct entropy calculation from computer simulation of liquids. *Phys. Rev. A* **1989**, *40*, 3817.

(26) Laird, B. B.; Haymet, A. Calculation of the entropy from multiparticle correlation functions. *Phys. Rev. A* **1992**, *45*, 5680.

(27) Karplus, M.; Kushick, J. N. Method for estimating the configurational entropy of macromolecules. *Macromolecules* **1981**, *14*, 325–332.

(28) Green, H. S. The molecular theory of fluids. **1952**,

(29) Wallace, D. C. Statistical theory for the entropy of a liquid. *Phys. Rev. A* **1989**, *39*, 4843.

(30) Li, G.; Liu, C.; Zhu, Z. Excess entropy scaling for transport coefficients: diffusion and viscosity in liquid metals. *J. Non-Cryst. Solids* **2005**, *351*, 946–950.

(31) Jakse, N.; Pasturel, A. Excess entropy scaling law for diffusivity in liquid metals. *Sci. Rep.* **2016**, *6*, 20689.

(32) Gao, M.; Widom, M. Information entropy of liquid metals. *The Journal of Physical Chemistry B* **2018**, *122*, 3550–3555.

(33) Desgranges, C.; Delhommelle, J. Unraveling liquid polymorphism in silicon driven out-of-equilibrium. *J. Chem. Phys.* **2020**, *153*, 054502.

(34) Zielkiewicz, J. Structural properties of water: Comparison of the SPC, SPCE, TIP4P, and TIP5P models of water. *J. Chem. Phys.* **2005**, *123*, 104501.

(35) Sharma, R.; Chakraborty, S. N.; Chakravarty, C. Entropy, diffusivity, and structural order in liquids with waterlike anomalies. *J. Chem. Phys.* **2006**, *125*, 204501.

(36) Errington, J. R.; Truskett, T. M.; Mittal, J. Excess-entropy-based anomalies for a waterlike fluid. *J. Chem. Phys.* **2006**, *125*, 244502.

(37) de Oliveira, A. B.; Franzese, G.; Netz, P. A.; Barbosa, M. C. Waterlike hierarchy of anomalies in a continuous spherical shouldered potential. *J. Chem. Phys.* **2008**, *128*, 064901.

(38) Giaquinta, P.; Giunta, G. About entropy and correlations in a fluid of hard spheres. *Physica A* **1992**, *187*, 145–158.

(39) Lazaridis, T.; Karplus, M. Orientational correlations and entropy in liquid water. *J. Chem. Phys.* **1996**, *105*, 4294–4316.

(40) Truskett, T.; Torquato, S.; Debenedetti, P. Towards a quantification of disorder in materials: Distinguishing equilibrium and glassy sphere packings. *Phys. Rev. E* **2000**, *62*, 993.

(41) Gnan, N.; Schrøder, T. B.; Pedersen, U. R.; Bailey, N. P.; Dyre, J. C. Pressure-energy correlations in liquids. IV.?Isomorphs? in liquid phase diagrams. *J. Chem. Phys.* **2009**, *131*, 234504.

(42) Tanaka, H. Bond orientational order in liquids: Towards a unified description of water-like anomalies, liquid-liquid transition, glass transition, and crystallization. *Eur. Phys. J. E* **2012**, *35*, 113.

(43) Lazaridis, T.; Paulaitis, M. E. Entropy of hydrophobic hydration: a new statistical mechanical formulation. *J. Phys. Chem.* **1992**, *96*, 3847–3855.

(44) Lazaridis, T.; Paulaitis, M. E. Simulation studies of the hydration entropy of simple, hydrophobic solutes. *J. Phys. Chem.* **1994**, *98*, 635–642.

(45) Ashbaugh, H. S.; Paulaitis, M. E. Entropy of hydrophobic hydration: Extension to hydrophobic chains. *J. Phys. Chem.* **1996**, *100*, 1900–1913.

(46) Young, T.; Abel, R.; Kim, B.; Berne, B. J.; Friesner, R. A. Motifs for molecular recognition exploiting hydrophobic enclosure in protein–ligand binding. *Proc. Natl. Acad. Sci. USA* **2007**, *104*, 808–813.

(47) Abel, R.; Young, T.; Farid, R.; Berne, B. J.; Friesner, R. A. Role of the active-site solvent in the thermodynamics of factor Xa ligand binding. *J. Am. Chem. Soc.* **2008**, *130*, 2817–2831.

(48) Baranyai, A.; Evans, D. J. Three-particle contribution to the configurational entropy of simple fluids. *Phys. Rev. A* **1990**, *42*, 849.

(49) Lin, S.-T.; Blanco, M.; Goddard III, W. A. The two-phase model for calculating thermodynamic properties of liquids from molecular dynamics: Validation for the phase diagram of Lennard-Jones fluids. *J. Chem. Phys.* **2003**, *119*, 11792–11805.

(50) Lin, S.-T.; Maiti, P. K.; Goddard III, W. A. Two-phase thermodynamic model for efficient and accurate absolute entropy of water from molecular dynamics simulations. *J. Phys. Chem. B* **2010**, *114*, 8191–8198.

(51) Desgranges, C.; Delhommelle, J. The central role of entropy in adiabatic ensembles and its application to phase transitions in the grand-isobaric adiabatic ensemble. *ArXiv e-prints* **2020**,

(52) Desgranges, C.; Delhommelle, J. Evaluation of the Grand-Canonical Partition Function using Expanded Wang-Landau Simulations. I. Thermodynamic Properties in the Bulk and at the Liquid-Vapor Phase Boundary. *J. Chem. Phys.* **2012**, *136*, 184107.

(53) Desgranges, C.; Delhommelle, J. Evaluation of the Grand-Canonical Partition Function using Expanded Wang-Landau Simulations. II. Adsorption of Atomic and Molecular Fluids in a Porous Material. *J. Chem. Phys.* **2012**, *136*, 184108.

(54) Desgranges, C.; Delhommelle, J. Evaluation of the Grand-Canonical Partition Function using Expanded Wang-Landau Simulations. III. Impact of combining rules on mixture properties. *J. Chem. Phys.* **2014**, *140*, 104109.

(55) Desgranges, C.; Delhommelle, J. Evaluation of the Grand-Canonical Partition Function using Expanded Wang-Landau Simulations. IV. Performance of many-body force fields and tight-binding schemes for the fluid phases of Silicon. *J. Chem. Phys.* **2016**, *144*, 124510.

(56) Desgranges, C.; Delhommelle, J. Evaluation of the grand-canonical partition function using expanded Wang-Landau simulations. V. Impact of an electric field on the thermodynamic properties and ideality contours of water. *J. Chem. Phys.* **2016**, *145*, 184504.

(57) Wang, F.; Landau, D. P. Determining the Density of States for Classical Statistical Models: A Random Walk Algorithm to produce a Flat Histogram. *Phys. Rev. E* **2001**, *64*, 056101.

(58) Wang, F.; Landau, D. Efficient, Multiple-Range Random Walk Algorithm to calculate the Density of States. *Phys. Rev. Lett.* **2001**, *86*, 2050–2053.

(59) Shell, M. S.; Debenedetti, P. G.; Panagiotopoulos, A. Z. Generalization of the Wang-Landau Method for Off-Lattice Simulations. *Phys. Rev. E* **2002**, *66*, 056703.

(60) Yan, Q.; Faller, R.; de Pablo, J. J. Density-of-States Monte Carlo Method for Simulation of Fluids. *J. Chem. Phys.* **2002**, *116*, 8745–8750.

(61) Ganzenmüller, G.; Camp, P. J. Applications of Wang-Landau Sampling to Determine Phase Equilibria in Complex Fluids. *J. Chem. Phys.* **2007**, *127*, 154504.

(62) Desgranges, C.; Delhommelle, J. Phase Equilibria of Molecular Fluids via Hybrid Monte Carlo Wang-Landau Simulations: Applications to Benzene and n-Alkanes. *J. Chem. Phys.* **2009**, *130*, 244109.

(63) Lyubartsev, A. P.; Martsinovski, A. A.; Shevkunov, S. V.; Vorontsov-Velyaminov, P. N. New Approach to Monte Carlo Calculation of the Free Energy: Method of Expanded Ensembles. *J. Chem. Phys.* **1992**, *96*, 1776–1783.

(64) Escobedo, F.; de Pablo, J. J. Expanded Grand Canonical and Gibbs Ensemble Monte Carlo Simulation of Polymers. *J. Chem. Phys.* **1996**, *105*, 4391.

(65) Muller, M.; Paul, W. Measuring the Chemical Potential of Polymer Solutions and Melts in Computer Simulations. *J. Chem. Phys.* **1994**, *100*, 719–724.

(66) Singh, J. K.; Errington, J. R. Calculation of Phase Coexistence Properties and Surface Tensions of n-Alkanes with Grand-Canonical Transition-Matrix Monte Carlo Simulation and Finite-Size Scaling. *J. Phys. Chem. B* **2006**, *110*, 1369–1376.

(67) Shi, W.; Maginn, E. J. Continuous Fractional Component Monte Carlo: An Adaptive Biasing Method for Open System Atomistic Simulations. *J. Chem. Theory Comput.* **2007**, *3*, 1451–1463.

(68) Rane, K. S.; Murali, S.; Errington, J. R. Monte Carlo Simulation Methods for Computing Liquid–Vapor Saturation Properties of Model Systems. *J. Chem. Theory Comput.* **2013**, *9*, 2552–2566.

(69) Desgranges, C.; Delhommelle, J. Many-body effects on the thermodynamics of fluids, mixtures and nanoconfined fluids. *J. Chem. Theory Comput.* **2015**, *11*, 5401.

(70) Desgranges, C.; Margo, A.; Delhommelle, J. Ideality contours and thermodynamic regularities in supercritical molecular fluids. *Chem. Phys. Lett.* **2016**, *658*, 37–42.

(71) Delhommelle, J. Etablissement de potentiels d'interaction pour la simulation moleculaire. Application a la prediction des equilibres liquide-vapeur de melanges binaires alcane-molecule multipolaire. Ph.D. thesis, Paris 11, 2000.

(72) Potoff, J. J.; Siepmann, J. I. Vapor–liquid equilibria of mixtures containing alkanes, carbon dioxide, and nitrogen. *AIChE J.* **2001**, *47*, 1676–1682.

(73) Allen, M. P.; Tildesley, D. J. *Computer Simulation of Liquids*; Clarendon Press, Oxford, 1987.

(74) Berendsen, H.; Grigera, J.; Straatsma, T. The missing term in effective pair potentials. *J. Phys. Chem.* **1987**, *91*, 6269–6271.

(75) Nezbeda, I.; Jirsák, J. Water and aqueous solutions: simple non-speculative model approach. *Phys. Chem. Chem. Phys.* **2011**, *13*, 19689–19703.

(76) Desgranges, C.; Delhommelle, J. Benchmark free energies and entropies for saturated and compressed water. *J. Chem. Eng. Data* **2017**, *62*, 4032–4040.

(77) Vargaftik, N. B.; Vinoradov, Y. K.; Yargin, V. S. *Handbook of Physical Properties of Liquids and Gases*; Begell House, New York, 1996.

(78) Wagner, W.; Pruß, A. The IAPWS formulation 1995 for the thermodynamic properties of ordinary water substance for general and scientific use. *J. Phys. Chem. Ref. Data* **2002**, *31*, 387–535.

(79) Widom, B.; Rowlinson, J. S. New model for the study of liquid–vapor phase transitions. *J. Chem. Phys.* **1970**, *52*, 1670–1684.

(80) Towns, J.; Cockerill, T.; Dahan, M.; Foster, I.; Gaither, K.; Grimshaw, A.; Hazlewood, V.; Lathrop, S.; Lifka, D.; Peterson, G. D. et al. XSEDE: Accelerating Scientific Discovery. *Computing in Science & Engineering* **2014**, *16*, 62–74.

TOC Graphic

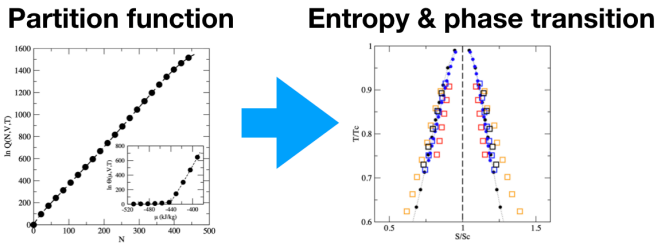
Partition function
Entropy & phase transition
ln Q(N,V,T)
N
T/Tc
S/Sc